







Cite this: *Nanoscale*, 2018, **10**, 22908

## Highly active single-layer MoS<sub>2</sub> catalysts synthesized by swift heavy ion irradiation†

Lukas Madauß, <sup>‡a</sup> Ioannis Zegkinoglou, <sup>‡b</sup> Henrique Vázquez Muiños,<sup>c</sup> Yong-Wook Choi,<sup>d</sup> Sebastian Kunze,<sup>b</sup> Meng-Qiang Zhao,<sup>d</sup> Carl H. Naylor,<sup>d</sup> Philipp Ernst,<sup>a</sup> Erik Pollmann,<sup>a</sup> Oliver Ochedowski,<sup>a</sup> Henning Lebius,<sup>e</sup> Abdenacer Benyagoub,<sup>e</sup> Brigitte Ban-d'Etat,<sup>e</sup> A. T. Charlie Johnson,<sup>d</sup> Flyura Djurabekova,<sup>c</sup> Beatriz Roldan Cuenya <sup>\*b,f</sup> and Marika Schleberger <sup>\*a</sup>

Two-dimensional molybdenum-disulfide (MoS<sub>2</sub>) catalysts can achieve high catalytic activity for the hydrogen evolution reaction upon appropriate modification of their surface. The intrinsic inertness of the compound's basal planes can be overcome by either increasing the number of catalytically active edge sites or by enhancing the activity of the basal planes *via* a controlled creation of sulfur vacancies. Here, we report a novel method of activating the MoS<sub>2</sub> surface using swift heavy ion irradiation. The creation of nanometer-scale structures by an ion beam, in combination with the partial sulfur depletion of the basal planes, leads to a large increase of the number of low-coordinated Mo atoms, which can form bonds with adsorbing species. This results in a decreased onset potential for hydrogen evolution, as well as in a significant enhancement of the electrochemical current density by over 160% as compared to an identical but non-irradiated MoS<sub>2</sub> surface.

Received 9th June 2018,  
Accepted 25th October 2018

DOI: 10.1039/c8nr04696d

rsc.li/nanoscale

## Introduction

The electrochemical evolution of H<sub>2</sub> from water (HER) is a promising clean solution to address the increasing global demand for energy. Among the possible electrocatalyst materials, platinum (Pt) and its alloys are the most efficient, requiring the lowest overpotential for the HER.<sup>1,2</sup> However, the high cost and low natural abundance of Pt encourage the search for alternative catalytic systems. The group of transition metal dichalcogenides (TMDCs) has attracted growing interest, mostly due to their extraordinary properties arising when their thickness is reduced to the nanoscale regime. In single-layer form, two-dimensional (2D) TMDCs exhibit distinct electronic properties, which strongly differ from those of their bulk counterparts.<sup>3–6</sup> The most famous representative of 2D TMDCs

is molybdenum disulfide (MoS<sub>2</sub>), which has been used in various applications in the fields of electronics,<sup>7</sup> optoelectronics<sup>8</sup> and catalysis.<sup>9–13</sup> Although the basal planes of single-layer MoS<sub>2</sub> (SLM) are inert due to their electronic structure and therefore not suitable for catalysis, their edges show an increased catalytic activity<sup>14–16</sup> for many important catalytic reactions, such as hydrodesulfurization,<sup>17,18</sup> oxygen reduction reactions<sup>19</sup> and the HER.<sup>10,11,15,20–23</sup>

So far, two general approaches have been followed to further optimize MoS<sub>2</sub> for the HER: (i) improving the intrinsic reactivity of MoS<sub>2</sub> by lowering the hydrogen binding energy<sup>20,24</sup> and (ii) increasing the total number of catalytically active sites.<sup>10–13</sup> The latter are low-coordinated Mo atoms either located at the edges of MoS<sub>2</sub> crystallites<sup>11</sup> or in the vicinity of sulfur (S) vacancies on the basal planes of MoS<sub>2</sub>.<sup>12</sup> Extensive synthesis and surface engineering efforts are usually required to achieve these goals. Some of the methods that have been suggested include the synthesis of three-dimensional (3D) shaped building blocks,<sup>10</sup> the growth of multi-layered MoS<sub>2</sub> sandwich structures,<sup>22</sup> and the doping of MoS<sub>2</sub> with metal nanoparticles.<sup>20</sup>

Because of the lower displacement threshold energy of S compared to Mo (roughly by a factor of six<sup>23</sup>), S may be selectively removed from MoS<sub>2</sub> by either electron or ion bombardment.<sup>11,12,25</sup> For ions with kinetic energies of up to a few 10 keV, the main interaction mechanism involves direct collisions between particles which result mainly in single or double S

<sup>a</sup>Faculty of Physics and CENIDE, Universität Duisburg-Essen, 47057 Duisburg, Germany. E-mail: marika.schleberger@uni-due.de

<sup>b</sup>Department of Physics, Ruhr-Universität Bochum, 44780 Bochum, Germany

<sup>c</sup>Department of Physics, University of Helsinki, P.O. Box 43, 00014 Helsinki, Finland

<sup>d</sup>Department of Physics and Astronomy, University of Pennsylvania, Philadelphia, USA

<sup>e</sup>CIMAP, (CEA-CNRS-ENSICAEN-UNICAEN), Blvd Henri Becquerel, Caen, France

<sup>f</sup>Department of Interface Science, Fritz-Haber Institute of the Max Planck Society, 14195 Berlin, Germany. E-mail: roldan@fhi-berlin.mpg.de

†Electronic supplementary information (ESI) available. See DOI: 10.1039/c8nr04696d

‡Both authors have contributed equally.



vacancies. Note that for 2D materials (in contrast to 3D materials) this limitation cannot be overcome by increasing the kinetic energy because collision cascades are absent in 2D materials. The efficiency is thus low, and as a consequence, a rather high fluence of roughly one incoming ion per removed S atom must be applied.

The alternative approach we present here is engineering defects *via* electronic energy deposition. This can be achieved by either highly charged or by very fast (swift) heavy ions. For both it has been shown that they can be used for defect engineering of 2D materials such as carbon nano-membranes,<sup>26,27</sup> graphene,<sup>28–33</sup> hexagonal boron nitride,<sup>34</sup> and MoS<sub>2</sub>.<sup>35–37</sup>

Swift heavy ions (SHI) excite target atoms along their trajectory and the corresponding energy deposited per track length into the target material is usually given in terms of electronic stopping power  $S_e = dE/dx$ . They offer an additional advantage that they are not stopped within a few nm as the ions in the keV range. Instead, their projected range extends up to several  $\mu\text{m}$  into the material. By using grazing incidence conditions, it is possible to bring a large part of this interaction volume to the surface.<sup>38,39</sup> In this way, every single ion modifies extended surface areas, which in the case of ultrathin MoS<sub>2</sub> leads to the creation of incisions, *i.e.* elongated interstices with parallel edges, which are hundreds of nm long and tens of nm wide.

This unique type of modification is due to a combination of direct energy deposition into MoS<sub>2</sub> and the interaction of the SHI with the substrate. As was shown earlier,<sup>37,39</sup> the dimensions of the nano-incisions agree well with the assumption that the energy transfer of the incident ion to the material can be described as a two-step process: first, the SHI excites the electronic system of the substrate material. In the second step, the energy is transferred *via* electron–phonon-coupling to the lattice, resulting in a so-called thermal spike in the substrate. This in turn leads to the decomposition of MoS<sub>2</sub> and in particular, the vaporization of S. The minimum energy deposited per track length for this process was found to be  $S_e = 2 \text{ keV nm}^{-1}$ .<sup>37</sup>

This work demonstrates by combining experiment and theory that SHI irradiation can be used to introduce artificial defects which enhance the catalytic activity. The SHI-induced defects include both nanometer-scale morphological features (such as incisions and Origami-like structures) and atomic scale lattice modifications (S vacancies). Both types of defects contribute to an increase of the concentration of low-coordinated Mo sites. Through the investigation of the role of defects in MoS<sub>2</sub> HER catalysts, a fundamental understanding of structure–reactivity correlations will be obtained.

## Results and discussion

High-quality monolayers of MoS<sub>2</sub> were synthesized by a chemical vapor deposition (CVD) process on SiO<sub>2</sub> substrates. Raman spectroscopy and photoluminescence (PL) measurements, Fig. 1(a), identified the material under investigation as single layer MoS<sub>2</sub> (SLM). This is evidenced by the characteristic A<sub>1g</sub>

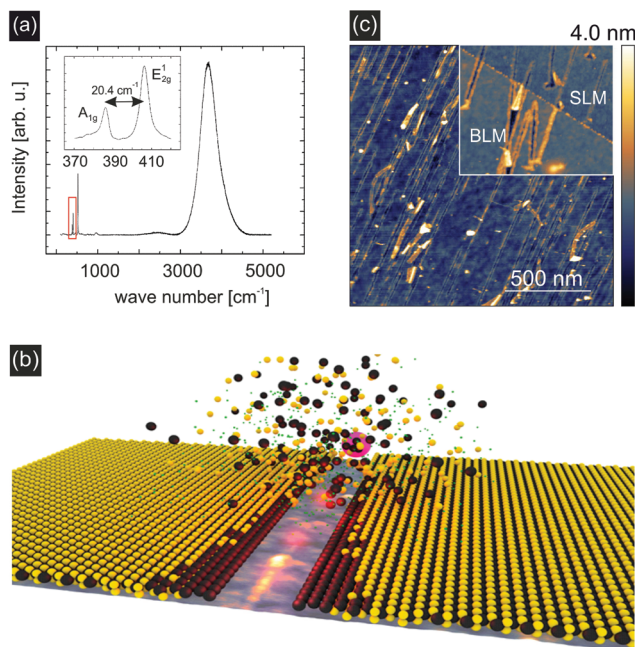


**Fig. 1** (a) Raman- and PL spectroscopy of pristine SLM. (b) Schematic illustration of rift formation with desulfurized low-coordinated Mo edges in MoS<sub>2</sub> on SiO<sub>2</sub> due to ion impact. (c) Atomic Force Microscopy (AFM) images after ion irradiation show the result of the ion impact under grazing incidence with respect to the MoS<sub>2</sub> surface. Elongated rifts in the MoS<sub>2</sub> are formed along the ion trajectory which increases the concentration of catalytically active edges. The inset presents an AFM topography image of single- and bilayer MoS<sub>2</sub> after exposure to air for an extended period of time.

and E<sub>2g</sub><sup>1</sup> lattice vibrations at wavenumbers of 385 cm<sup>-1</sup> and 405 cm<sup>-1</sup> (ref. 5) and the pronounced PL feature at 4000 cm<sup>-1</sup>. The latter also demonstrates a high degree of crystallinity<sup>6</sup> (see Fig. S1 for Raman and PL mappings of irradiated and non-irradiated MoS<sub>2</sub> in the ESI†). The MoS<sub>2</sub> monolayers were subsequently transferred onto glassy carbon (GC) substrates by applying a PMMA transfer technique. For further details on the growth and transfer process see the ESI.†

Fig. 1(b) schematically illustrates the mechanism of defect formation in MoS<sub>2</sub> by SHI irradiation. The removal of material around the ion track leaves edges behind consisting of under-coordinated Mo atoms. Furthermore, due to the thermal spike induced by the ion, also adjacent S atoms are likely to evaporate during the process. Both the low-coordinated Mo atoms at the edges of the nano-incisions and the additional S vacancies are expected to contribute to the catalytic activity. Atomic force microscopy (AFM) images of SHI irradiated MoS<sub>2</sub> samples, acquired after exposure of the samples to air for extended periods of time, show that the edges of the incisions are heavily decorated with adsorbates, see the inset of Fig. 1(c). This is an indication of an enhanced chemical reactivity and is also found for bilayer MoS<sub>2</sub> (BLM) samples.

To test our hypothesis and to investigate the catalytic activity of our defect-engineered samples in detail we irradiated SLM with 91 MeV Xe ions under grazing incidence at an



angle of  $\theta = 1^\circ$  with respect to the surface and with a fluence (number of ions per area) of 15 ions per  $\mu\text{m}^2$ . The corresponding energy deposited per track length was  $S_e = 19 \text{ keV nm}^{-1}$  into  $\text{MoS}_2$ ,  $S_e = 12 \text{ keV nm}^{-1}$  into  $\text{SiO}_2$ , and  $S_e = 9.3 \text{ keV nm}^{-1}$  into glassy carbon.<sup>40</sup> AFM images were obtained on irradiated samples directly after irradiation, see Fig. 1(c). The AFM images reveal elongated irradiation induced incisions in the  $\text{MoS}_2$  with an average length of  $400 \text{ nm} \pm 200 \text{ nm}$  on  $\text{SiO}_2$  (at  $1^\circ$  ion incidence with respect to the surface). Assuming that the edges are completely desulfurized we would arrive at an upper limit for the efficiency of  $\sim 4800 \text{ S atoms per incident ion}$ , which corresponds to a sulfur vacancy density of *ca.*  $7.2 \times 10^4 \mu\text{m}^{-2}$  for these given irradiation parameters. It should be noted that the length and the density of the incisions can be easily controlled during irradiation by varying the angle with respect to the surface and choosing a higher or lower ion fluence, respectively. At too high fluences however, tracks will start to overlap so that the achievable sulfur vacancy density will saturate at some stage.

The effect of ion irradiation on the morphology of the samples is also evident in scanning electron microscopy (SEM) images. Representative examples of both irradiated and non-irradiated  $\text{MoS}_2$  surfaces on GC are shown in Fig. 2. In addition to the incisions that are formed along the direction of the ion beam, three-dimensional structures with typical sizes of a few dozens of nm are also formed due to the bombard-

ment of the surface with SHI. The latter consist of folded material and are a result of two incisions running very close to each other.<sup>37</sup> These “Origami-like” structures exhibit a large surface area and a large number of edge sites and are thus expected to be beneficial for the catalytic activity of the material. From a comparison of SHI induced incisions in  $\text{MoS}_2$  deposited on  $\text{SiO}_2$  (Fig. 1) and on glassy carbon, (Fig. 2), it becomes evident that both exhibit similar morphological properties. We can thus infer that the creation mechanism is the same for the two substrates. No SHI-induced three-dimensional structures were observed in areas of the glassy carbon substrate surface which were not covered by a single layer of  $\text{MoS}_2$  (Fig. S3†). Thus, these morphological features are characteristic of the  $\text{MoS}_2$  system and not of the underlying support.

To obtain a microscopic image of the ion induced modifications, we performed molecular dynamics (MD) simulations. Irradiation was simulated with the inelastic thermal spike model<sup>41,42</sup> on unsupported  $\text{MoS}_2$  under grazing incidence ( $1^\circ$  with respect to the surface) for 91 MeV Xe ions. Note that the dimensions of the sheet were  $200 \times 40 \text{ nm}^2$  (for details see the ESI†), considerably shorter than the length of the incisions as measured in the experiments.

The results are shown in Fig. 3. One can easily recognize the nano-incision in the  $\text{MoS}_2$  layer, which has two amorphous edges running parallel to each other, similar to the features seen in the AFM and SEM images in Fig. 1 and 2. The amorphization along the trajectory in Fig. 3(a) and (b) impedes the quantification of the relationship between the catalytic activity and the structural changes related to low-coordinated Mo atoms and sulfur vacancies. We therefore plotted the result in a different way by removing all sputtered Mo and S atoms from the simulation box, together with the amorphous chains on the edges, see Fig. 3(c) and (d). Here, the color of the Mo

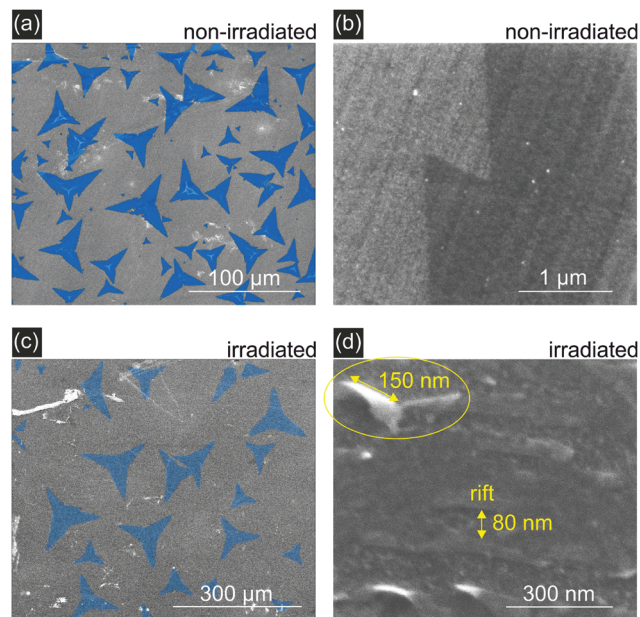


**Fig. 2** SEM images of non-irradiated (a), (b) and ion-irradiated (c), (d)  $\text{MoS}_2$  monolayers deposited on GC. The irradiated surface exhibits nanometer-scale morphological features, such as incisions ( $\sim 80 \text{ nm}$  wide and several  $\mu\text{m}$  long) and three-dimensional “Origami-like” structures (see the example in the circle and ESI Fig. S2 and S3†), which are characterized by a large number of under-coordinated edge sites. The non-irradiated surfaces are flat and featureless except for the intrinsic roughness of the glassy carbon substrate. The  $\text{MoS}_2$  areas in (a) and (c) are highlighted in blue. The marked sample regions are used in the calculation of the geometric surface area.

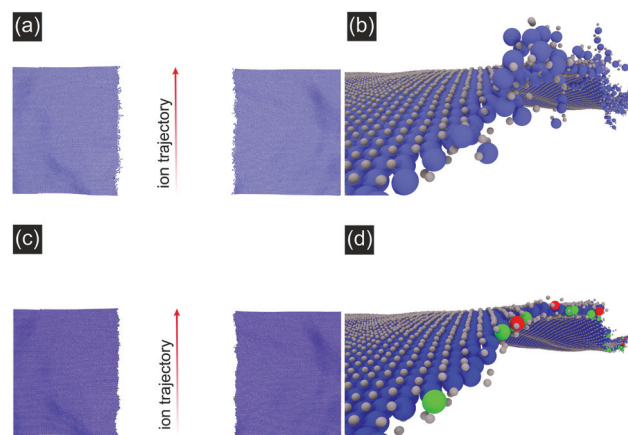


**Fig. 3** Molecular dynamics simulations of a suspended single-layer  $\text{MoS}_2$  sheet irradiated with 91 MeV Xe ions under a grazing incidence of  $1^\circ$  with respect to the surface. (a), (b) An incision with amorphized edges running along the ion trajectory is shown. (c), (d) For easier quantification, sputtered Mo and S atoms have been removed, together with the amorphous chains and the coordination number of the remaining Mo atoms has been color coded. Blue: Mo atoms with a coordination number of 6; green: 5, red: 4.





atoms corresponds to their coordination number (blue = coordination number of 6, green = coordination number of 5, red = coordination number of 4). The obtained MD data suggest that on each side of the incision roughly 29% of adjacent S atoms are missing and that 28% of the edge Mo atoms are under-coordinated (higher if the amorphous chains are also considered). This means we have to refine our initial estimate of the irradiation efficiency to approximately 1400 S atoms per incident ion, corresponding to a sulfur vacancy density of *ca.*  $2.1 \times 10^4 \mu\text{m}^{-2}$  at an ion fluence of  $15 \mu\text{m}^{-2}$ .

The width of the incision in the MD simulations is smaller ( $\sim 40$  nm) in comparison with the experiment ( $\sim 80$  nm) probably due to neglecting the role of the substrate, which can create defects in the MoS<sub>2</sub> in two ways. First, particles may be sputtered from the substrate resulting in further damage. This effect is assumed to be small in our case, as the cross section for nuclear stopping is negligible for SHI. However, the substrate will be heated by the thermal spike and this may also give rise to further damage. This effect cannot be neglected, in particular as the direct interaction of the beam with the 2D material is limited to a few 10 nm depending on the angle of incidence but the incisions can be much longer, *i.e.* a few 100 nm.

We therefore investigated the effect of the thermal spike in the substrate by applying the Two-Temperature Model (TTM).<sup>37–39</sup> This model assumes that the energy deposited into the electronic system is transferred into the phonon system. The flow of energy from the electronic to the phonon system depends on the temperature difference between the two reservoirs and is governed by the electron–phonon-coupling constant of the material. Solving the two coupled heat diffusion equations yields spatial temperature profiles from which one can estimate whether a specific phase transition of the material occurs or not (see the ESI† for more details).

The calculated temperature profile for the SiO<sub>2</sub> substrate irradiated with 91 MeV Xe ( $S_e = 12.3 \text{ keV nm}^{-1}$ ) is shown in Fig. 4. The white dotted lines depict the isotherm at 1458 K which is the decomposition temperature of MoS<sub>2</sub>.<sup>43,44</sup> The required temperature for evaporation of S is even lower, *e.g.* S<sub>2</sub> evaporates at 1140 K and in the presence of water already at 565 K by vaporizing as SO<sub>2</sub>. This indicates that indeed the substrate plays an important role for the formation of incisions. Note that we did not simulate the different substrates used for this study as we expect no significant differences in the mechanism. Quantitative differences such as deposited energy and length of incisions do exist between the different substrates. The defect creation mechanism is expected to be the same though.

As the simulations support our interpretation that catalytically active sites are indeed efficiently created by SHI irradiation we investigated our samples using X-ray photoelectron spectroscopy (XPS) to obtain information on the elemental composition and chemical state of the catalyst surface. The data for non-irradiated and irradiated MoS<sub>2</sub> samples (the same irradiation conditions as before) are shown in Fig. 5. In both cases we measured a signal originating from

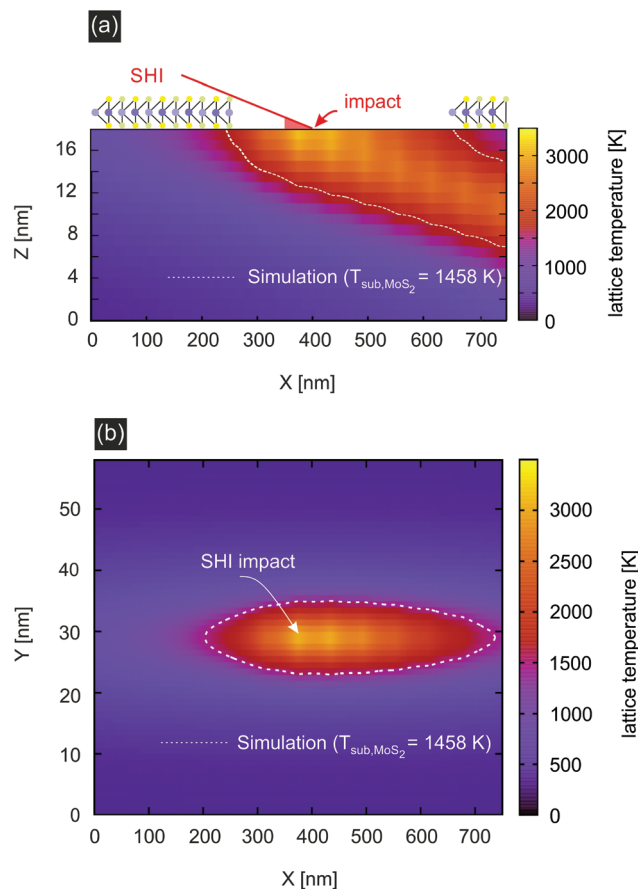
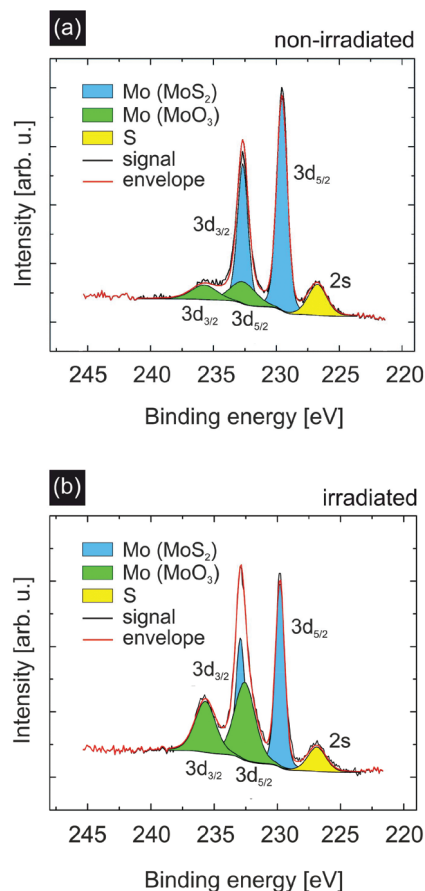


Fig. 4 Calculated temperature profile (a) side and (b) top view in the SiO<sub>2</sub> substrate after irradiation with 91 MeV Xe ions under a grazing incidence of 1° with respect to the surface. The white dotted line depicts the isotherm at the decomposition temperature of MoS<sub>2</sub>.

the Mo 3d<sub>5/2</sub> and Mo 3d<sub>3/2</sub> peaks of MoS<sub>2</sub> (blue) and MoO<sub>3</sub> (green).<sup>45</sup> In the case of non-irradiated MoS<sub>2</sub> (Fig. 5(a)) the MoO<sub>3</sub> contributes  $\sim 20\%$  to the overall Mo signal. This can be attributed to the already oxidized edges of the grown MoS<sub>2</sub> flakes as for the XPS measurements the samples had to be exposed to ambient conditions. After irradiation, however, the MoO<sub>3</sub> constitutes  $\sim 49\%$  of the overall Mo signal. We can easily explain this by assuming that the edges of the incisions created by ions in MoS<sub>2</sub> provide additional catalytically active low-coordinated Mo atoms which are likely to oxidize when exposed to air.<sup>46</sup>

Apart from these low-coordinated Mo atoms, we argue that SHI irradiation also creates S vacancies next to the incisions due to the thermal spike after ion impact because the lower sublimation temperature of S compared to Mo results in a preferential evaporation of S atoms in adjacent rows next to the ion trajectory. When analyzing the stoichiometry of Mo and S in the XPS data prior to and after irradiation using the XPS peak areas and the corresponding relative sensitivity factors (RSFs),<sup>47</sup> we indeed see a clear increase of the total Mo:S ratio. Whereas the Mo(MoS<sub>2</sub>):S ratio does not change upon irradiation maintaining its initial value of 0.45 (corresponding





**Fig. 5** XPS spectra of non-irradiated (a) and ion-irradiated (b) single layer MoS<sub>2</sub>. The irradiation was performed with 91 MeV Xe ions under a grazing incidence of 1° with respect to the surface. One can observe a strong increase of the Mo signal originating from MoO<sub>3</sub> for irradiated MoS<sub>2</sub>. Also, the intensity ratio of Mo/S (we refer here to the total Mo amount of both MoS<sub>2</sub> and MoO<sub>3</sub>) strongly increases which can be explained by a lower sublimation temperature of S than Mo.

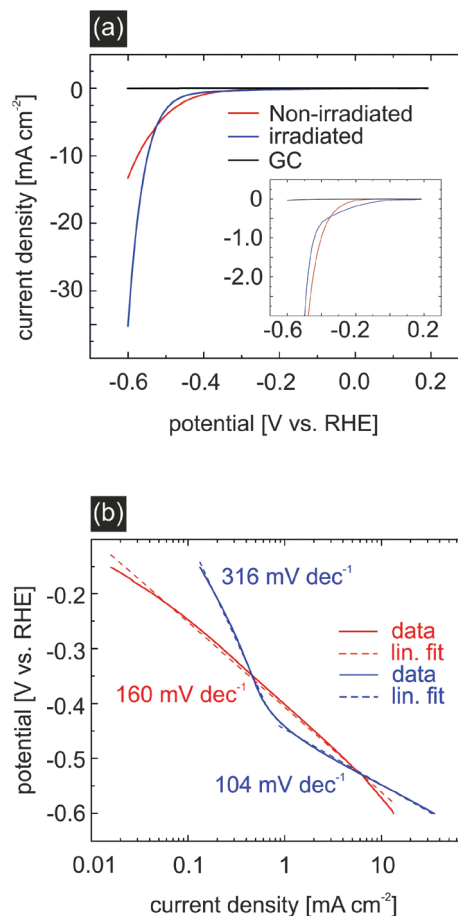


**Fig. 6** HER measurements of non-irradiated (red) and irradiated (blue) MoS<sub>2</sub>. Glassy carbon (GC) has been used as a substrate (black). Ion fluence was chosen as 40 ions per  $\mu\text{m}^2$ . (a) Current density as a function of the potential [V vs. RHE] shows strong activity enhancement of irradiated MoS<sub>2</sub> compared to non-irradiated MoS<sub>2</sub>. The inset of (a) shows the less negative onset potential for irradiated MoS<sub>2</sub>. (b)  $V$ - $I$  curves with Tafel-slopes of irradiated (blue) and non-irradiated (red) MoS<sub>2</sub>.

to an atomic composition of Mo<sub>0.91</sub>S<sub>2</sub>, the total Mo(MoS<sub>2</sub> + MoO<sub>3</sub>):S ratio strongly increases from 0.56 to 0.88. In agreement with our hypothesis it is the significant increase of the MoO<sub>3</sub> concentration which leads to the change in stoichiometry. Since SHI irradiation creates S vacancies, which are occupied by O atoms upon exposure of the sample to air, the increase of the amount of oxides in the XPS spectra after irradiation reflects the higher concentration of S vacancies (compared to the non-irradiated sample) prior to exposure to air. At least part of these O-filled vacancies becomes unoccupied again under the reducing conditions of the HER, thus contributing to the catalytic activity. Further XPS data and analysis can be found in the ESI.†

To test the extent to which the ion irradiation influences the catalytic activity of MoS<sub>2</sub>, we performed linear sweep voltammetry (LSV) measurements on non-irradiated and irradiated MoS<sub>2</sub> in an aqueous 0.5 M H<sub>2</sub>SO<sub>4</sub> solution (Fig. 6(a)). For these experiments glassy carbon was chosen as a substrate due to its high conductivity and inert behaviour during hydro-

gen evolution reaction (HER) measurements. The ion fluence for glassy carbon/MoS<sub>2</sub> samples used for electrochemical characterization was chosen slightly higher, *i.e.* 40 ions per  $\mu\text{m}^2$ , while the angle of incidence was kept at 1°. From the AFM analysis these parameters were estimated to yield a sufficiently high sulfur vacancy density without compromising sample integrity due to excessive overlapping of rifts. At a potential of  $-0.6$  V vs. RHE, non-irradiated MoS<sub>2</sub> (red curve) displays a current density of  $-13.3$  mA cm<sup>-2</sup>, whereas irradiated MoS<sub>2</sub> (blue curve) exhibits an almost three times higher current density of  $-35.3$  mA cm<sup>-2</sup>. Large current values at low applied voltages are desirable for the HER as this qualifies the material under investigation as a suitable catalyst.

Another important characteristic of an efficient catalyst is the onset potential, which determines the necessary energy input to initiate the hydrogen evolution. It corresponds to the Gibbs free energy  $\Delta G_{\text{H}}$  of hydrogen bonding to the catalytic sites of MoS<sub>2</sub>.<sup>14,48</sup> A large deviation from this value will lead to



a too strong/too weak hydrogen adsorption which negatively affects the hydrogen desorption and electron–proton transfer, respectively, and ultimately the catalytic activity. It is therefore desirable to have materials with a  $\Delta G_{\text{H}}$  close to zero. In our experiment, we measured for pristine MoS<sub>2</sub> an onset potential of  $-220$  mV, which is consistent with previous studies for nanostructured MoS<sub>2</sub>.<sup>10,15,16,48,49</sup> For ion irradiated MoS<sub>2</sub> there is a strong indication that the onset potential decreases, *e.g.* in order to obtain a current density of  $200 \mu\text{A cm}^{-2}$ , the applied potential for non-irradiated MoS<sub>2</sub> was  $-300$  mV, whereas the potential for irradiated MoS<sub>2</sub> was just  $-200$  mV. This observation is in accordance with the work performed by Li *et al.*<sup>50</sup> who theoretically increased the number of S vacancies, hence obtaining a minimum in  $\Delta G_{\text{H}}$  of approx.  $0.02$  eV at a S-vacancy density of 12.5%. In our experiment, the introduction of S vacancies and S-depleted regions is due to a thermal effect resulting from a heated substrate track along the ion trajectory as shown in TTM simulations and XPS data. Note, that determining an exact value of the onset potential for irradiated MoS<sub>2</sub> is rather difficult due to possible non-faradaic behaviour at low currents.

We further analyzed the Tafel-slope and the exchange current density, see Fig. 6(b). The Tafel-slope can be viewed as a measure of the reaction kinetics. It is desirable that the value of the Tafel-slope is as low as possible.<sup>51,52</sup>

$$\ln(-j) = \ln(j_0) - \eta/b \quad (1)$$

Here,  $j$  represents the current density,  $j_0$  is the exchange current density,  $b$  is the Tafel slope, and  $\eta$  is the overpotential. In the case of non-irradiated MoS<sub>2</sub>, we measured a Tafel-slope of  $160 \text{ mV dec}^{-1}$  which is slightly larger compared to values reported in the literature. Irradiated MoS<sub>2</sub> however displays two independent regions with different Tafel-slopes, both differing from the slope of the non-irradiated MoS<sub>2</sub> sample. The region with a slope of  $316 \text{ mV dec}^{-1}$  is likely affected by capacitance effects and shall not be considered further. For applied potentials more negative than  $-0.4 \text{ V vs. RHE}$  we measured a Tafel-slope of  $104 \text{ mV dec}^{-1}$ , which is in good agreement with the values reported in the literature for MoS<sub>2</sub>.<sup>9,10,15,16,22,24,53</sup> The smaller Tafel slope as compared to the non-irradiated sample is also an indication of improved catalytic properties upon SHI treatment.

The exchange current density should in principle be determined by linear extrapolation of the Tafel plot in the low potential region, *i.e.* where the Tafel slope for the irradiated MoS<sub>2</sub> is equal to  $316 \text{ mV dec}^{-1}$  (Fig. 6). However, since this region is likely affected by capacitance effects, the exchange current density determined in this way would be overestimated.

Because our catalytic material is purely two-dimensional every part of the MoS<sub>2</sub> is in direct contact with the GC electrode which positively contributes to an efficient electron transfer (see Fig. S5 in the ESI†). Apart from the morphological changes induced by the ion irradiation, a reaction promoting effect is also expected as a result of desulfurization of the basal planes, in line with our MD and XPS data. This effect

has been previously seen also for keV Ar<sup>+</sup> beam irradiation experiments and corroborated by *ab initio* molecular dynamics simulations.<sup>54,55</sup> The important role of S vacancies in the HER catalytic activity of TMDCs has also been recently demonstrated for bulk pentlandite (Fe<sub>4.5</sub>Ni<sub>4.5</sub>S<sub>8</sub>) materials.<sup>56,57</sup> Given that the concentration of S vacancies changes during the reaction and that the interplay between desulfurization and subsequent protonation is dependent on the applied potential, a systematic study of the S vacancy effect on the catalytic activity would require operando spectroscopic studies, which are beyond the scope of this work.

## Conclusion

Single layers of MoS<sub>2</sub> have been synthesized *via* chemical vapor deposition and irradiated with swift heavy ions under grazing incidence. *Via* this defect-engineering approach, catalytically active low-coordinated Mo atoms along the incisions edges of 3D structures, as well as S depleted regions could be created. Furthermore, the density of such sites can be easily controlled by varying the irradiation parameters. We observed a strong enhancement of the catalytic activity by  $\sim 160\%$  as well as indications of a lowered onset potential for irradiated MoS<sub>2</sub>. Our approach constitutes an effective alternative for increasing the catalytic activity of MoS<sub>2</sub> because it involves neither a complex synthesis procedure nor a preparation process with ligands. In contrast to other techniques, which use 3D catalysts, our 2D MoS<sub>2</sub> catalysts promote an effective electron transfer since every part of the MoS<sub>2</sub> is in direct contact with the GC substrate, hence minimizing charge transfer resistance. Due to the low threshold for creating incisions in MoS<sub>2</sub> when irradiated under grazing incidence, also smaller accelerators are suitable for this defect engineering strategy. Our approach thus represents a major step towards the fundamental understanding of the role of rationally designed defects in the activity of MoS<sub>2</sub> catalysts for HER applications.

## Conflicts of interest

There are no conflicts to declare.

## Acknowledgements

M. S. and L. M. acknowledge funding of the NU-TEGRAM project within the FLAG-ERA program by the Deutsche Forschungsgemeinschaft (DFG) (SCHL 384/16-1). B. R. C., I. Z., and Y.-W. C. acknowledge financial support from the Cluster of Excellence RESOLV at RUB (EXC 1096), funded by the DFG. S. K. acknowledges financial support from the Max Planck Research School for Interface Controlled Materials for Energy Conversion (IMPRS-SurMat). M. Q. Z., C. H. N., and A. T. C. H. acknowledge the support from the U.S. National Science Foundation (NSF) Grant EFRI 2-DARE 1542879.



We thank U. Hagemann from the Interdisciplinary Center for Analytics on the Nanoscale (ICAN, core facility funded by the German Research Foundation, DFG) for support with the XPS measurements.

## Notes and references

- H. B. Gray, Powering the planet with solar fuel, *Nat. Chem.*, 2009, **1**, 112.
- A. B. Laursen, S. Kegnæs, S. Dahl and I. Chorkendorff, Molybdenum sulfides—efficient and viable materials for electro- and photoelectrocatalytic hydrogen evolution, *Energy Environ. Sci.*, 2012, **5**, 5577.
- S. Bertolazzi, J. Brivio and A. Kis, Stretching and breaking of ultrathin MoS<sub>2</sub>, *ACS Nano*, 2011, **5**, 9703–9709.
- G. R. Bhimanapati, Z. Lin, V. Meunier, Y. Jung, J. Cha, S. Das, Di Xiao, Y. Son, M. S. Strano, V. R. Cooper, L. Liang, S. G. Louie, E. Ringe, W. Zhou, S. S. Kim, R. R. Naik, B. G. Sumpter, H. Terrones, F. Xia, Y. Wang, J. Zhu, D. Akinwande, N. Alem, J. A. Schuller, R. E. Schaak, M. Terrones and J. A. Robinson, Recent Advances in Two-Dimensional Materials beyond Graphene, *ACS Nano*, 2015, **9**, 11509–11539.
- C. Lee, H. Yan, L. E. Brus, T. F. Heinz, J. Hone and S. Ryu, Anomalous lattice vibrations of single- and few-layer MoS<sub>2</sub>, *ACS Nano*, 2010, **4**, 2695–2700.
- A. Splendiani, L. Sun, Y. Zhang, T. Li, J. Kim, C.-Y. Chim, G. Galli and F. Wang, Emerging photoluminescence in monolayer MoS<sub>2</sub>, *Nano Lett.*, 2010, **10**, 1271–1275.
- D. Lembke and A. Kis, Breakdown of high-performance monolayer MoS<sub>2</sub> transistors, *ACS Nano*, 2012, **6**, 10070–10075.
- O. Lopez-Sanchez, D. Lembke, M. Kayci, A. Radenovic and A. Kis, Ultrasensitive photodetectors based on monolayer MoS<sub>2</sub>, *Nat. Nanotechnol.*, 2013, **8**, 497–501.
- D. Merki and X. Hu, Recent developments of molybdenum and tungsten sulfides as hydrogen evolution catalysts, *Energy Environ. Sci.*, 2011, **4**, 3878.
- J. Kibsgaard, Z. Chen, B. N. Reinecke and T. F. Jaramillo, Engineering the surface structure of MoS<sub>2</sub> to preferentially expose active edge sites for electrocatalysis, *Nat. Mater.*, 2012, **11**, 963–969.
- G. Li, Du Zhang, Q. Qiao, Y. Yu, D. Peterson, A. Zafar, R. Kumar, S. Curtarolo, F. Hunte, S. Shannon, Y. Zhu, W. Yang and L. Cao, All The Catalytic Active Sites of MoS<sub>2</sub> for Hydrogen Evolution, *J. Am. Chem. Soc.*, 2016, **138**, 16632–16638.
- Y. Yin, J. Han, Y. Zhang, X. Zhang, P. Xu, Q. Yuan, L. Samad, X. Wang, Y. Wang, Z. Zhang, P. Zhang, X. Cao, B. Song and S. Jin, Contributions of Phase, Sulfur Vacancies, and Edges to the Hydrogen Evolution Reaction Catalytic Activity of Porous Molybdenum Disulfide Nanosheets, *J. Am. Chem. Soc.*, 2016, **138**, 7965–7972.
- J. Xie, J. Zhang, S. Li, F. Grote, X. Zhang, H. Zhang, R. Wang, Y. Lei, B. Pan and Y. Xie, Controllable disorder engineering in oxygen-incorporated MoS<sub>2</sub> ultrathin nanosheets for efficient hydrogen evolution, *J. Am. Chem. Soc.*, 2013, **135**, 17881–17888.
- B. Hinnemann, P. G. Moses, J. Bonde, K. P. Jørgensen, J. H. Nielsen, S. Horch, I. Chorkendorff and J. K. Nørskov, Biomimetic hydrogen evolution, *J. Am. Chem. Soc.*, 2005, **127**, 5308–5309.
- T. F. Jaramillo, K. P. Jørgensen, J. Bonde and J. H. Nielsen, Identification of Active Edge Sites for Electrochemical H<sub>2</sub> Evolution from MoS<sub>2</sub> Nanocatalysts, *Science*, 2007, 100–102.
- J. Bonde, P. G. Moses, T. F. Jaramillo, J. K. Nørskov and I. Chorkendorff, Hydrogen evolution on nano-particulate transition metal sulfides, *Faraday Discuss.*, 2008, **140**, 219–231.
- W. P. Boone and J. G. Ekerdt, Hydrodesulfurization Studies with a Single-Layer Molybdenum Disulfide Catalyst, *J. Catal.*, 2000, **193**, 96–102.
- B. Salmeron and G. A. Somorjai, The Adsorption and Binding of Thiophene, Butene and H<sub>2</sub>S on the Basal Plane of MoS<sub>2</sub> Single Crystals, *Chem. Phys. Lett.*, 1982, **90**, 105–107.
- S. M. Ahmed and H. Gerischer, Influence of Crystal Surface Orientation on Redox Reactions at Semiconducting MoS<sub>2</sub>, *Electrochim. Acta*, 1987, **24**, 705–711.
- X. Dai, K. Du, Z. Li, M. Liu, Y. Ma, H. Sun, X. Zhang and Y. Yang, Co-Doped MoS<sub>2</sub> Nanosheets with the Dominant CoMoS Phase Coated on Carbon as an Excellent Electrocatalyst for Hydrogen Evolution, *ACS Appl. Mater. Interfaces*, 2015, **7**, 27242–27253.
- M.-R. Gao, M. K. Y. Chan and Y. Sun, Edge-terminated molybdenum disulfide with a 9.4 Å interlayer spacing for electrochemical hydrogen production, *Nat. Commun.*, 2015, **6**, 7493.
- D. Kong, H. Wang, J. J. Cha, M. Pasta, K. J. Koski, J. Yao and Y. Cui, Synthesis of MoS<sub>2</sub> and MoSe<sub>2</sub> films with vertically aligned layers, *Nano Lett.*, 2013, **13**, 1341–1347.
- M. Ghorbani-Asl, S. Kretschmer, D. E. Spearot and A. V. Krashennnikov, Two-dimensional MoS<sub>2</sub> under ion irradiation, *2D Mater.*, 2017, **4**, 25078.
- Y. Li, H. Wang, L. Xie, Y. Liang, G. Hong and H. Dai, MoS<sub>2</sub> nanoparticles grown on graphene, *J. Am. Chem. Soc.*, 2011, **133**, 7296–7299.
- S. Bertolazzi, S. Bonacchi, G. Nan, A. Pershin, D. Beljonne and P. Samori, Engineering Chemically Active Defects in Monolayer MoS<sub>2</sub> Transistors via Ion-Beam Irradiation and Their Healing via Vapor Deposition of Alkanethiols, *Adv. Mater.*, 2017, **29**, 1606760.
- R. A. Wilhelm, E. Gruber, R. Ritter, R. Heller, A. Beyer, A. Turchanin, N. Klingner, R. Hübner, M. Stöger-Pollach, H. Vieker, G. Hlawacek, A. Götzhäuser, S. Facsko and F. Aumayr, Threshold and efficiency for perforation of 1 nm thick carbon nanomembranes with slow highly charged ions, *2D Mater.*, 2015, **2**, 35009.
- R. A. Wilhelm, E. Gruber, R. Ritter, R. Heller, S. Facsko and F. Aumayr, Charge exchange and energy loss of slow highly





- charged ions in 1 nm thick carbon nanomembranes, *Phys. Rev. Lett.*, 2014, **112**, 153201.
- 28 S. Akcöltekin, H. Bukowska, T. Peters, O. Osmani, I. Monnet, I. Alzahr, B. B. d'Etat, H. Lebius and M. Schleberger, Unzipping and folding of graphene by swift heavy ions, *Appl. Phys. Lett.*, 2011, **98**, 103103.
- 29 J. Hopster, R. Kozubek, B. Ban-d'Etat, S. Guillous, H. Lebius and M. Schleberger, Damage in graphene due to electronic excitation induced by highly charged ions, *2D Mater.*, 2014, **1**, 11011.
- 30 O. Ochedowski, O. Lehtinen, U. Kaiser, A. Turchanin, B. Ban-d'Etat, H. Lebius, M. Karlušić, M. Jakšić and M. Schleberger, Nanostructuring graphene by dense electronic excitation, *Nanotechnol.*, 2015, **26**, 465302.
- 31 H. Vázquez, E. H. Åhlgren, O. Ochedowski, A. A. Leino, R. Mirzayev, R. Kozubek, H. Lebius, M. Karlušić, M. Jakšić, A. V. Krashennnikov, J. Kotakoski, M. Schleberger, K. Nordlund and F. Djurabekova, Creating nanoporous graphene with swift heavy ions, *Carbon*, 2017, **114**, 511–518.
- 32 L. Madauß, J. Schumacher, M. Ghosh, O. Ochedowski, J. Meyer, H. Lebius, B. Ban-d'Etat, M. E. Toimil-Molares, C. Trautmann, R. G. H. Lammertink, M. Ulbricht and M. Schleberger, Fabrication of nanoporous graphene/polymer composite membranes, *Nanoscale*, 2017, **9**, 10487–10493.
- 33 W. Li, X. Wang, X. Zhang, S. Zhao, H. Duan and J. Xue, Mechanism of the defect formation in supported graphene by energetic heavy ion irradiation, *Sci. Rep.*, 2015, **5**, 9935.
- 34 R. Kozubek, P. Ernst, C. Herbig, T. Michely and M. Schleberger, Fabrication of Defective Single Layers of Hexagonal Boron Nitride on Various Supports for Potential Applications in Catalysis and DNA Sequencing, *ACS Appl. Nano Mater.*, 2018, **1**, 3765–3773.
- 35 O. Ochedowski, K. Marinov, G. Wilbs, G. Keller, N. Scheuschner, D. Severin, M. Bender, J. Maultzsch, F. J. Tegude and M. Schleberger, Radiation hardness of graphene and MoS<sub>2</sub> field effect devices against swift heavy ion irradiation, *J. Appl. Phys.*, 2013, **113**, 214306.
- 36 J. Hopster, R. Kozubek, J. Krämer, V. Sokolovsky and M. Schleberger, Ultra-thin MoS<sub>2</sub> irradiated with highly charged ions, *Nucl. Instrum. Methods Phys. Res., Sect. B*, 2013, **317**, 165–169.
- 37 L. Madauß, O. Ochedowski, H. Lebius, B. Ban-d'Etat, C. H. Naylor, A. T. C. Johnson, J. Kotakoski and M. Schleberger, Defect engineering of single- and few-layer MoS<sub>2</sub> by swift heavy ion irradiation, *2D Mater.*, 2017, **4**, 15034.
- 38 E. Akcöltekin, T. Peters, R. Meyer, A. Duvenbeck, M. Klusmann, I. Monnet, H. Lebius and M. Schleberger, Creation of multiple nanodots by single ions, *Nat. Nanotechnol.*, 2007, **2**, 290–294.
- 39 O. Ochedowski, O. Osmani, M. Schade, B. K. Bussmann, B. Ban-d'Etat, H. Lebius and M. Schleberger, Graphitic nanostripes in silicon carbide surfaces created by swift heavy ion irradiation, *Nat. Commun.*, 2014, **5**, 3913.
- 40 J. F. Ziegler, M. D. Ziegler and J. P. Biersack, SRIM – The stopping and range of ions in matter (2010), *Nucl. Instrum. Methods Phys. Res., Sect. B*, 2010, **268**, 1818–1823.
- 41 G. Szenes, Comparison of two thermal spike models for ion–solid interaction, *Nucl. Instrum. Methods Phys. Res., Sect. B*, 2011, **269**, 174–179.
- 42 C. Trautmann, S. Klaumünzer and H. Trinkaus, Effect of stress on track formation in morphous iron boron alloy Ion tracks as elastic inclusions, *Phys. Rev. Lett.*, 2000, **85**, 3648–3651.
- 43 R. Yang, Z. Liu, Y. Wang, G. Yang and H. Li, Synthesis and characterization of MoS<sub>2</sub>/Ti composite coatings on Ti6Al4 V prepared by laser cladding, *AIP Adv.*, 2013, **3**, 22106.
- 44 J. M. Gordon, E. A. Katz, D. Feuermann, A. Albu-Yaron, M. Levy and R. Tenne, Singular MoS<sub>2</sub>, SiO<sub>2</sub> and Si nanostructures—synthesis by solar ablation, *J. Mater. Chem.*, 2008, **18**, 458–462.
- 45 D. Ganta, S. Sinha and R. T. Haasch, 2-D Material Molybdenum Disulfide Analyzed by XPS, *Surf. Sci. Spectra*, 2014, **21**, 19–27.
- 46 H. Guo, Y. Sun, P. Zhai, H. Yao, J. Zeng, S. Zhang, J. Duan, M. Hou, M. Khan and J. Liu, Swift-heavy ion irradiation-induced latent tracks in few- and mono-layer MoS<sub>2</sub>, *Appl. Phys. A*, 2016, **122**, 463.
- 47 C. D. Wagner, Sensitivity factors for XPS analysis of surface atoms, *J. Electron Spectrosc. Relat. Phenom.*, 1983, **32**, 99–102.
- 48 J. Greeley, T. F. Jaramillo, J. Bonde, I. B. Chorkendorff and J. K. Nørskov, Computational high-throughput screening of electrocatalytic materials for hydrogen evolution, *Nat. Mater.*, 2006, **5**, 909–913.
- 49 T. F. Jaramillo, J. Bonde, J. Zhang, B.-L. Ooi, K. Andersson, J. Ulstrup and I. Chorkendorff, Hydrogen Evolution on Supported Incomplete Cubane-type [Mo<sub>3</sub>S<sub>4</sub>]<sup>4+</sup> Electrocatalysts, *J. Phys. Chem. C*, 2008, **112**, 17492–17498.
- 50 H. Li, C. Tsai, A. L. Koh, L. Cai, A. W. Contryman, A. H. Fragapane, J. Zhao, H. S. Han, H. C. Manoharan, F. Abild-Pedersen, J. K. Nørskov and X. Zheng, Activating and optimizing MoS<sub>2</sub> basal planes for hydrogen evolution through the formation of strained sulphur vacancies, *Nat. Mater.*, 2016, **15**, 48–53.
- 51 L. Liao, J. Zhu, X. Bian, L. Zhu, M. D. Scanlon, H. H. Girault and B. Liu, MoS<sub>2</sub> Formed on Mesoporous Graphene as a Highly Active Catalyst for Hydrogen Evolution, *Adv. Funct. Mater.*, 2013, **23**, 5326–5333.
- 52 P. Atkins and J. D. Paula, *Atkin's Physical Chemistry*, Oxford University Press, GB, 7th edn, 2002.
- 53 Z. Chen, D. Cummins, B. N. Reinecke, E. Clark, M. K. Sunkara and T. F. Jaramillo, Core-shell MoO<sub>3</sub>-MoS<sub>2</sub> nanowires for hydrogen evolution, *Nano Lett.*, 2011, **11**, 4168–4175.
- 54 D. Le, T. B. Rawal and T. S. Rahman, Single-Layer MoS<sub>2</sub> with Sulfur Vacancies, *J. Phys. Chem. C*, 2014, **118**, 5346–5351.
- 55 Q. Ma, P. M. Odenthal, J. Mann, D. Le, C. S. Wang, Y. Zhu, T. Chen, D. Sun, K. Yamaguchi, T. Tran, M. Wurch,





- J. L. McKinley, J. Wyrick, K. Magnone, T. F. Heinz, T. S. Rahman, R. Kawakami and L. Bartels, Controlled argon beam-induced desulfurization of monolayer molybdenum disulfide, *J. Phys.: Condens. Matter*, 2013, **25**, 252201.
- 56 B. Konkana, K. Junge Puring, I. Sinev, S. Piontek, O. Khavryuchenko, J. P. Dürholt, R. Schmid, H. Tüysüz, M. Muhler, W. Schuhmann and U.-P. Apfel, Pentlandite rocks as sustainable and stable efficient electrocatalysts for hydrogen generation, *Nat. Commun.*, 2016, **7**, 12269.
- 57 I. Zegkinoglou, A. Zendegani, I. Sinev, S. Kunze, H. Mistry, H. S. Jeon, J. Zhao, M. Y. Hu, E. E. Alp, S. Piontek, M. Smialkowski, U.-P. Apfel, F. Körmann, J. Neugebauer, T. Hickel and B. Roldan Cuenya, Operando Phonon Studies of the Protonation Mechanism in Highly Active Hydrogen Evolution Reaction Pentlandite Catalysts, *J. Am. Chem. Soc.*, 2017, **139**, 14360–14363.

